S. Burton, N. Makris, I. Konstantopoulos and P.J. Antsaklis, "Modeling the Response of an Electrorheological Damper: Phenomenology and Emulation," J ournal o f E ngineering M echanics , pp. 897-906, September 1996.

MODELING THE RESPONSE OF ER DAMPER: PHENOMENOLOGY AND EMULATION

By Scott A. Burton,[1] Nicos Makris,[2] Member, ASCE, I. Konstantopoulos,[3] and P. J. Antsaklis[4]

ABSTRACT: In this paper physically motivated and nonparametric models are investigated that predict within some tolerance the response of a semiactive electrorheological (ER) damper that was designed, constructed, and tested. The electrorheological damper is a hydraulic device that was designed for applications in vibration control of civil structures. The simplest possible physically motivated phenomenological models are first considered to predict the damper response without and with the presence of electric field. Subsequently, the performance of a multilayer neural network constructed and trained by an efficient algorithm known as the dependence identification algorithm is examined to predict the response of the ER damper. The performance of the neural network is compared to that of the phenomenological models and some conclusions are provided.

INTRODUCTION

Semiactive dampers for vibration control of structures combine the advantages of passive structural control (Constantinou and Symans 1993) with the benefits of active structural control (Housner et al. 1994) to produce optimal, yet stable and reliable damping systems. Different types of semiactive dampers have been proposed ranging from simple electrorheological dampers (Stevens et al. 1984) to hydraulic dampers with mechanically controlled orificing (Kawashima and Unjoh 1994; Patten et al. 1994; Symans and Constantinou 1995).

Electrorheological (ER) dampers have attracted considerable attention in the last decade for vibration control of mechanical and structural systems. Early studies by Stevens et al. (1984) showed how a simple ER damper is capable of reducing displacement amplitudes when electric field is applied. ER dampers have found various applications in the automotive industry (Douclos 1988). Recently, ER dampers received considerable attention for vibration control of civil structures. The attraction of ER dampers is that they do not involve moving parts to control the fluid flow, and they are relatively inexpensive compared to hydraulic dampers with mechanically controlled orificing. Ehrgott and Masri (1992) presented identification techniques to model the behavior of a small ER damper that operates under shear flow. Gavin and Hanson (1994a,b) designed and tested an ER damper that consists of a rectangular container and a moving plunger comprised of nine flat parallel plates that are rigidly interconnected. In the study reported herein, the damper under investigation generates flow through a stationary annular duct, which is also known as Hagen Poiseille flow.

Recently, a prototype semiactive damper for seismic protection of structures was designed, constructed, and tested at the University of Notre Dame (Makris et al. 1996). The proposed damper is an electrorheological fluid damper that can deliver relatively large forces and has potential to be used for seismic and vibration protection of civil structures. A photograph of the constructed damper is shown in Fig. 1, and a schematic of its design is shown in Fig. 2. The damper consists of an outer cylinder and a double-ended piston rod that pushes the ER fluid through a stationary annular duct. The electric field is created perpendicular to the fluid flow.

Modeling the response of semiactive dampers is a key issue in the design and implementation of these devices in civil structures. Modeling procedures can range from numerical solutions of continuum mechanics equations to macroscopic input-output relations. Modeling procedures that are based on continuum mechanics are obtained by solving the balance of momentum and continuity equations together with some constitutive equation for the behavior of a material point within the damper. Such procedures can be computationally intense, but they are very useful for design of optimal geometries, since they reveal information about the deformation and flow of the materials used (Makris et al. 1993, 1995a,b). While mechanical models that are based on first principles provide insight on the mechanics that govern the response of a device, they are not practical for control purposes. Structural control engineers are primarily interested in macroscopic models that describe the response of the damper at the force-displacement level. Macroscopic models can vary from physically motivated mechanical models to nonparametric models used for pattern recognition or function approximation (artificial neural networks). The problem of developing the best macroscopic model that predicts the response of a structural or mechanical system is that it does not have a unique solution. Poincare (1929) pointed out that if a physical phenomenon can be represented by one mechanical model it can be represented by many other models. Thus, "springs," "dashpots" and "slid-

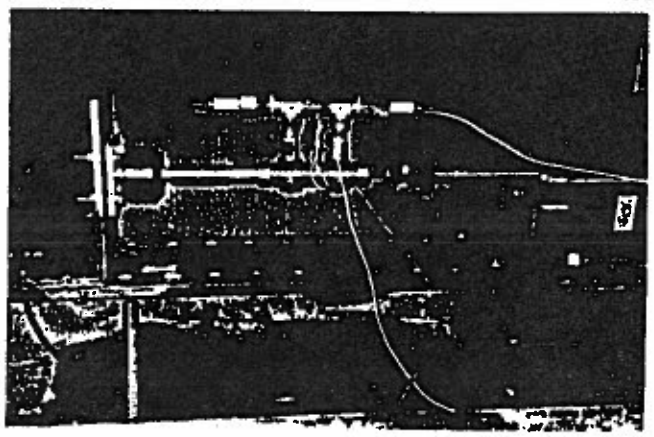

FIG. 1. Constructed Electrorheological Damper and Testing Arrangement

[1]Grad. Res. Asst., Dept. of Civ. Engrg. and Geological Sci., Univ. of Notre Dame, Notre Dame, IN 46556.
[2]Asst. Prof., Dept. of Civ. Engrg. and Geological Sci., Univ. of Notre Dame, Notre Dame, IN.
[3]Grad. Res. Asst., Dept. of Electr. Engrg., Univ. of Notre Dame, Notre Dame, IN.
[4]Prof., Dept. of Electr. Engrg., Univ. of Notre Dame, Notre Dame, IN.

Note. Associate Editor: Nicholas P. Jones. Discussion open until February 1, 1997. To extend the closing date one month, a written request must be filed with the ASCE Manager of Journals. The manuscript for this paper was submitted for review and possible publication on May 12, 1995. This paper is part of the *Journal of Engineering Mechanics*, Vol. 122, No. 9, September, 1996. ©ASCE, ISSN 0733-9399/96/0009-0000–0000/$4.00 + $.50 per page. Paper No. 10705.

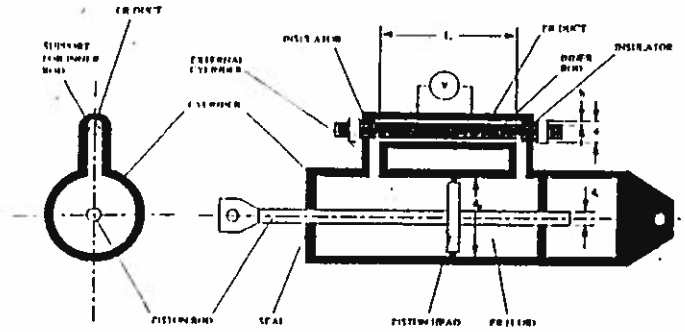

FIG. 2. Schematic of Proposed Electrorheological Fluid Damper

ers'' could be arranged in many different patterns, with all of them being equivalent (Shames and Cozzarelli 1992).

This paper first examines the performance of the simplest possible phenomenological models to predict the response of the electrorheological damper in the absence and presence of electric field ($E = 0$ and $E = 3$ kV/mm, respectively). Subsequently, the performance of a neural network that was constructed and trained to characterize the response of the damper is examined. Neural networks have been used with success in various civil engineering applications, such as predicting the spatial distribution of earthquake intensity (Tung et al. 1994) or actively controlling the response of structures (Ghaboussi and Joghataie 1995). A theoretical study on the modeling of mechanical behavior using neural networks has been presented by Masri et al. (1993).

ELECTRORHEOLOGICAL FLUID

The phenomenon of electrorheology was first reported by Winslow (1949) and characterized the considerable variation of rheological properties of some fluids when an electric field is applied. The manifested resistance to flow depends on the nature of the fluid, the conditions of flow, and the orientation and strength of the applied electric field. In some cases, the complete conversion from liquid to solid behavior is achieved in which a finite yield stress τ_y has to be exceeded to produce flow. When the latter is the case, it can be said that under the presence of electric field these ''fluids'' become ''solids,'' and they behave elastically when stressed at stresses smaller than the ''yield'' stress. Recent reviews on the phenomenon of electrorheology and its applications has been presented by Block and Kelly (1988) and Jordan and Shaw (1989).

The ER fluid within the damper consists of a carrier that is silicone oil with specific density 0.970, and the suspended solid that is zeolite with concentration 46% by weight. Oscillatory viscometric tests under the presence of electric field demonstrated that the silicon oil-zeolite mixture manifests more pronounced electrorheological properties than a similar mineral-oil-based mixture studied by Gamota and Filisco (1991) and Gamota et al. (1993).

Fig. 3 shows shear stress versus shear-strain-rate curves from steady viscometric tests at different values of the applied electric field on the ER fluid used within the damper. The yield stress of the ER fluid depends strongly on the electric field. At 3 kV/mm, the average value of the yield stress, τ_y is of the order of 1.4 kPa (0.20 psi). The zero-shear-rate viscosity increases gradually with electric field with a value of $\eta_0 \sim 7$ Pa·s at $E = 0$ to a value of $\eta_0 \sim 13.2$ Pa·s at 3 kV/mm.

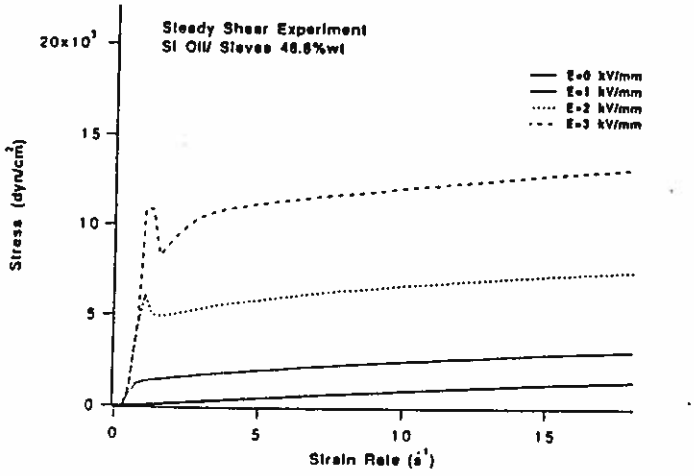

FIG. 3. Recorded Stress of ER Material under Steady Shear (0.1 Pa = 1 dyne/cm²)

EXPERIMENTAL PROGRAM

To calibrate, train, and validate the parametric phenomenological models and the nonparametric neural-network models under investigation, a series of harmonic and transient motions (earthquake motions) have been induced to the damper and the resulting response was measured. Dynamic testing of the damper was conducted using the arrangement shown in Fig. 1. A hydraulic actuator imposes a prescribed displacement history along the axis of the damper. The force developed in the damper is measured through a stationary load cell that is connected between the damper and the reaction frame (left end in Fig. 1). The displacement of the damper is measured using a LVDT linear variable differential transducer (LVDT) that is located within the actuator.

The electric field on the ER duct is applied through the cathode connected at the right end of the inner cylinder of the bypass shown in Fig. 1. The ''ground'' wire is connected at the center of the outer cylinder of the bypass. The third wire shown in Fig. 1 is connected to a temperature transducer (thermocouple) to monitor the temperature of the fluid along the bypass. This temperature exceeds the temperature of the main cylinder of the damper, since fluid velocities along the bypass are larger than elsewhere. The recorded temperature should not exceed the value of approximately 240°C (450°F) to prevent damage of the insulators. The recorded temperature during all experiments was approximately 26.5°C (80°F).

Fig. 4 shows a recorded force-displacement loop (dotted line) at very small piston velocities with $E = 0$. At the reversal of motion, one observes a net force drop of approximately 180

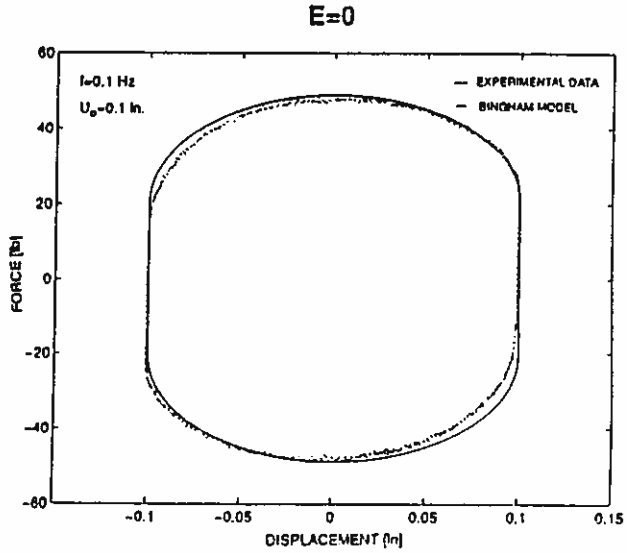

FIG. 4. Recorded and Predicted Force Displacement Loop from ER Damper at Small Piston Velocity (25.4 mm = 1 in.; 4.448 N = 1 lb)

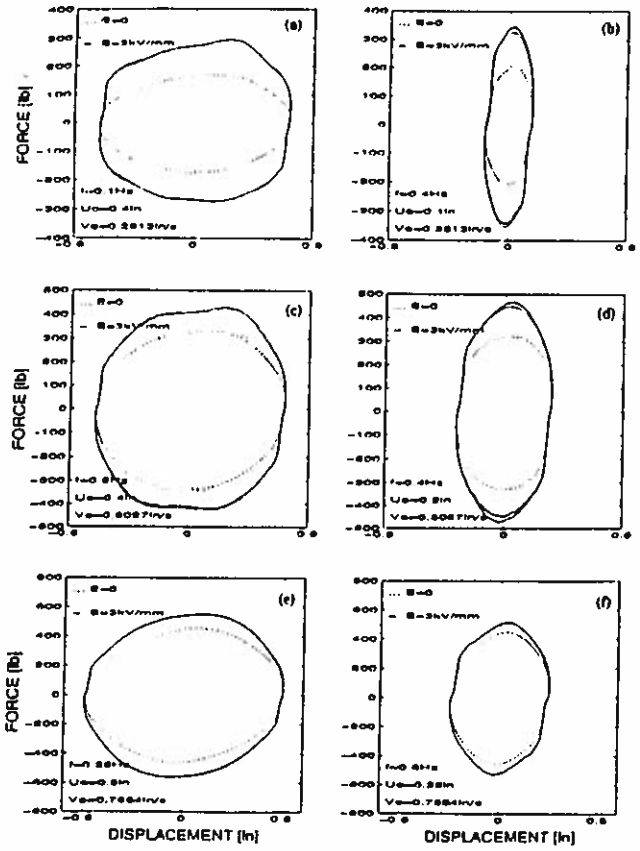

FIG. 5. Recorded Force-Displacement Loops from ER Damper at [illegible] (25.4 mm = 1 in.; 4.448 N = 1 lb)

Different Piston Velocities

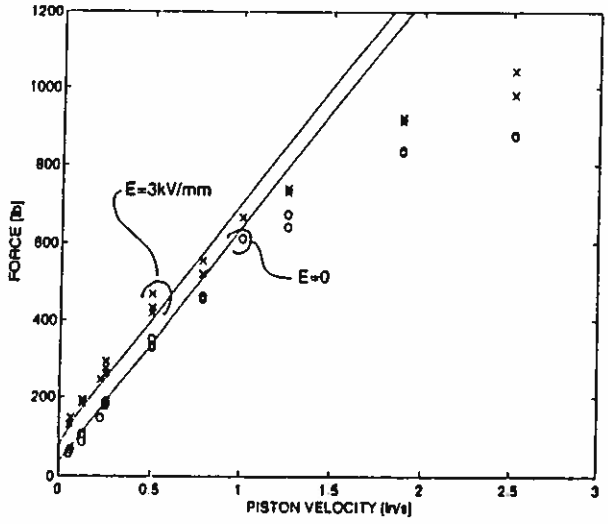

FIG. 6. Recorded Amplitudes of Piston Force as Function of Piston Velocity Amplitude (Circles: $E = 0$; Stars: $E = 3.0$ kV/mm) (25.4 mm = 1 in.; 4.448 N = 1 lb)

N (40 lb). This force drop is due to the friction force that the damper seals apply on the piston rod. This friction force is present in all experiments and its value is approximately 90 N.

Fig. 5 shows recorded force-displacement loops without electric field ($E = 0$) and with $E = 3$ kV/mm. At no electric field the recorded loops are nearly elliptical, whereas at $E = 3$ kV/mm some nonlinear behavior becomes apparent. As the piston velocity increases, viscous effects dominate over plastic effects, and the fraction of the force that can be controlled reduces. Fig. 5 also shows that the damper response is nearly frequency independent but strongly velocity dependent.

Viscous heating is, in general, an important issue for the design of dampers. In the case of seismic protection, dampers are subjected in most cases to a small number of cycles. For instance, in the case of an earthquake with approximate duration of 30 s, the number of significant cycles is between 10 and 20, and it is assumed that viscous heating is insufficient to considerably reduce the fluid viscosity. Moreover, the dampers are usually placed in the interior of the structure where the ambient temperature is controlled. In this study we do not examine the temperature dependence of the damper response. Nevertheless, viscous heating is an important problem that deserves a separate systematic investigation.

Fig. 6 shows the amplitudes of recorded force versus maximum piston velocity at no field (circles) and at $E = 3$ kV/mm (stars). The scatter in the data is due to viscous heating during testing. As the harmonic tests were conducted one after the other, the damper was subjected to many cycles and in some tests the temperature along the bypass was higher than along others, ranging from 75°F to 85°F. At zero field and small piston velocities the damper operates like a textbook-case dashpot, where the force is linearly proportional to the velocity. The small-velocity damping constant, C, can be computed from the Hagen-Poisseille flow theory (Schlichting 1987)

$$C = \frac{12\eta_0 L}{\pi d h^3} A_p^2 \tag{1}$$

where A_p = piston-head area. With reference to Fig. 2, the geometric characteristics of the constructed damper are $L = 54.6$ mm, $d = 14.3$ mm, $h = 0.8$ mm, $d_p = 33.4$ mm, and $d_r = 11.25$ mm. With these values and $\eta_0 \sim 7$ Pa·sec (see Fig. 3), the resulting value of $C = 122$ kN s/m ($C = 700$ lb s/in.), which is approximately the slope of the data at small piston velocities. Consequently, Fig. 6 shows that the Hagen-Poiseille theory (solid lines) predicts very well the damper response for piston velocities less than 15 mm/s (0.6 in./s). The finite value of force at zero velocity and $E = 0$ is due to the friction force that the seals exert on the rod.

At higher piston velocities the damper delivers a force proportional to the velocity raised at a power that is less than one [$F(t) = C(du/dt)^\alpha$, $0 < \alpha < 1$]. This desirable behavior is achieved because the piston head has a small orifice that allows for some flow at high piston velocities. The orifice utilizes a specially shaped passage to alter flow characteristics with fluid speed (Constantinou and Symans 1993). The reduction of the damping coefficient of the damper as piston velocity increases shows that at higher velocities the damper manifests some elasticity. Oscillatory tests have been conducted on the damper and the dynamic stiffness of the damping was extracted from measured force-displacement loops. Within the context of equivalent linear analysis, Fig. 7 (left side) plots as a function of frequency the storage stiffness, $K_1(\omega)$ and damping coefficient, $C(\omega)$, computed as

$$K_1(\omega) = \sqrt{\left(\frac{P_0}{u_0}\right)^2 - [\omega C(\omega)]^2}; \quad C(\omega) = \frac{W_D}{\pi \omega u_0^2} \tag{2a,b}$$

where u_0 = amplitude of imposed displacement; P_0 = amplitude of recorded force; ω = excitation frequency; and w_D = energy dissipated per cycle. At the zero-frequency limit the elasticity of the device is zero, whereas the experimental values for C present significant scatter. This scatter is the result of dividing two very small quantities [see (2)]. Fig. 7 (right side) plots the same information as Fig. 7 (left side), but the dynamic stiffness is expressed in terms of amplitude and phase.

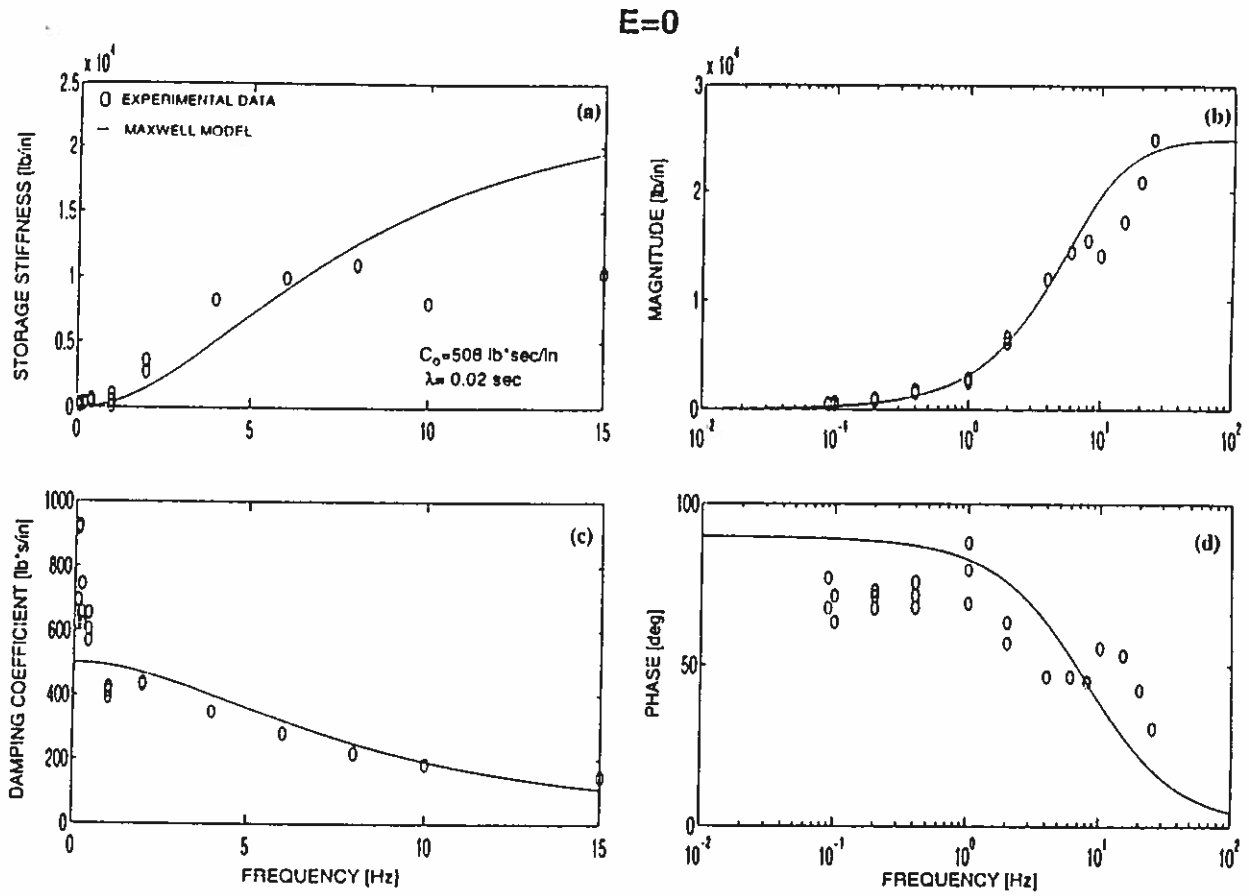

FIG. 7. Experimentally Measured Storage Stiffness and Damping Coefficient (Left), and Magnitude and Phase (Right) of ER Damper as Function of Frequency at $E = 0$ (Points); Solid Lines: Prediction of Maxwell Model (C = 506 lb s/in.; λ 0.02 s; 25.4 mm = 1 in.; 4.448 N = 1 lb)

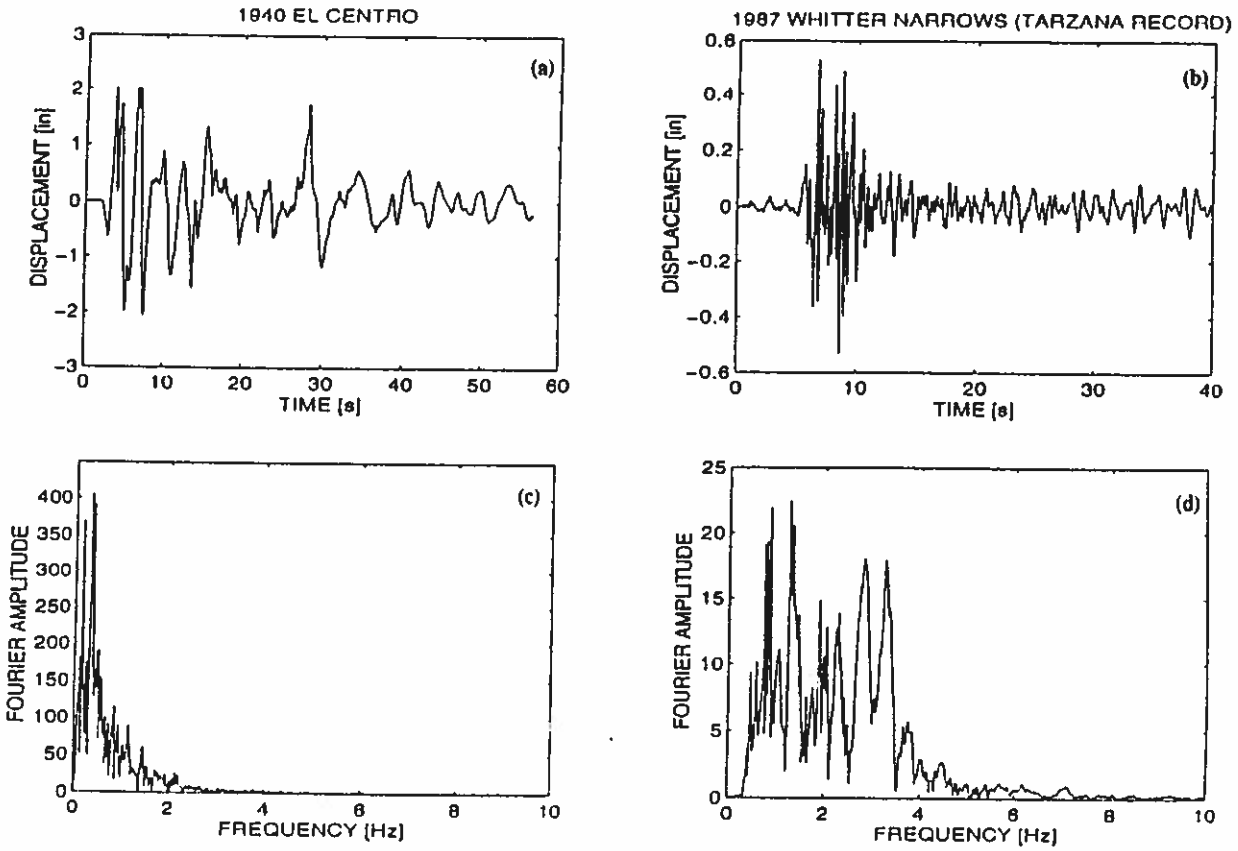

FIG. 8. Displacement Records and Fourier Amplitude Spectra from 1940 El Centro and 1987 Whittier Narrows Earthquake

PHENOMENOLOGICAL CONSTITUTIVE MODELS

The force-velocity correlation in Fig. 6 suggests that at the small-velocity range the piston force is proportional to the piston velocity. The total force on the piston is the result of the viscous forces due to the fluid flow plus the friction force, P_f, on the damper seals. A macroscopic model that includes both contributions is the viscoplastic Bingham model (Shames and Cozzarelli 1992)

$$P(t) = P_f \operatorname{sgn}(\dot{u}) + C\dot{u} \tag{3}$$

Of course, this purely dissipative model results in a zero storage stiffness and an equivalent linear damping coefficient with constant value. According to Fig. 7, the proposed Bingham model will be realistic at the low-frequency limit only. Indeed, the prediction of the calibrated Bingham model [C = 84 kN s/m (480 lb/in.), P_f = 90 N (20 lb)] satisfactorily predicts the recorded force-displacement loop shown in Fig. 4. Fig. 8 plots the time history (top) and the Fourier spectrum (bottom) of the 1940 El Centro earthquake (left side) and the 1987 Whittier Narrows earthquake-Tarzana record (right side). Obviously, the Bingham model neglects the increase in elasticity and the reduction in damping of the device at higher frequencies. Nevertheless, even for the Tarzana record, the high-frequency content beyond 5 Hz is not dominant and the Bingham model can be used as a first approximation to model the damper response. Fig. 9 (top left) compares the prediction of the Bingham model with the experimentally recorded force from the damper when subjected to the El Centro displacement history shown in this figure. The agreement is satisfactory. The top right plot in Fig. 9 shows the difference in the signal between the predicted and experimentally recorded force histories. This difference signal has a peak value (PV) of 200 lb and a root-mean-square (RMS) value of 32 lb. The RMS value of the signal is defined as

$$\text{RMS} = \sqrt{\frac{1}{N}\sum_{i=1}^{N}(P_{Ri} - P_{Pi})^2} \tag{4}$$

with $\mathbf{P}_R$ and $\mathbf{P}_P$ being vectors of recorded and predicted forces, respectively.

The ~~most~~ simplest model that can approximate the frequency dependence of the storage modulus and damping coefficient shown in Fig. 7 is the classical Maxwell model of viscoelasticity (Shames and Cozzarelli 1992)

$$P(t) + \lambda \frac{dP(t)}{dt} = C\frac{du(t)}{dt} \tag{5}$$

The Maxwell model is a linear viscoelastic model; therefore, is capable of capturing some of the elasticity that the damper manifests at higher frequencies. On the other hand, in the model given by (5), the friction force, P_f, is not expressed explicitly. The solid lines in Fig. 7 are the prediction of (5) with zero-frequency-damping constant, C = 88.6 kN/m (C = 506 lb s/in.) and relaxation time λ = 0.02 s. Fig. 9 (center-left) compares the prediction of the Maxwell model given by (5) with the experimentally measured force from the damper when subjected to the El Centro displacement history shown in Fig. 8. The prediction of the response is more favorable compared to the prediction from the Bingham model. The center-right plot in Fig. 9 shows the difference in the signal between the predicted and experimentally recorded force histories. Evidently, because of the presence of the relaxation term in the Maxwell model, the difference signal is more suppressed with a PV = 640 N (144 lb), and an RMS = 120 N (27 lb).

The performance of phenomenological models can be improved by adding terms on either side of the constitutive equation. For instance, the Bingham and Maxwell models can be combined in one constitutive equation.

$$P(t) + \lambda \frac{dP(t)}{dt} = C\frac{du(t)}{dt} + P_f \operatorname{sgn}(\dot{u}) \tag{6}$$

to capture both nonlinear and relaxation effects. Alternatively, within the context of equivalent linearization one can construct higher order linear models with higher order derivatives of the force and displacement (Franklin et al. 1991), or even fractional order derivatives (Makris and Constantinou 1991) to approximate the response within a smaller tolerance. The parameters of such models do not have direct physical meaning; however, higher order models might be more appropriate for control purposes. In the next section we examine the performance of a neural network that is a more general model to approximate input-output relations.

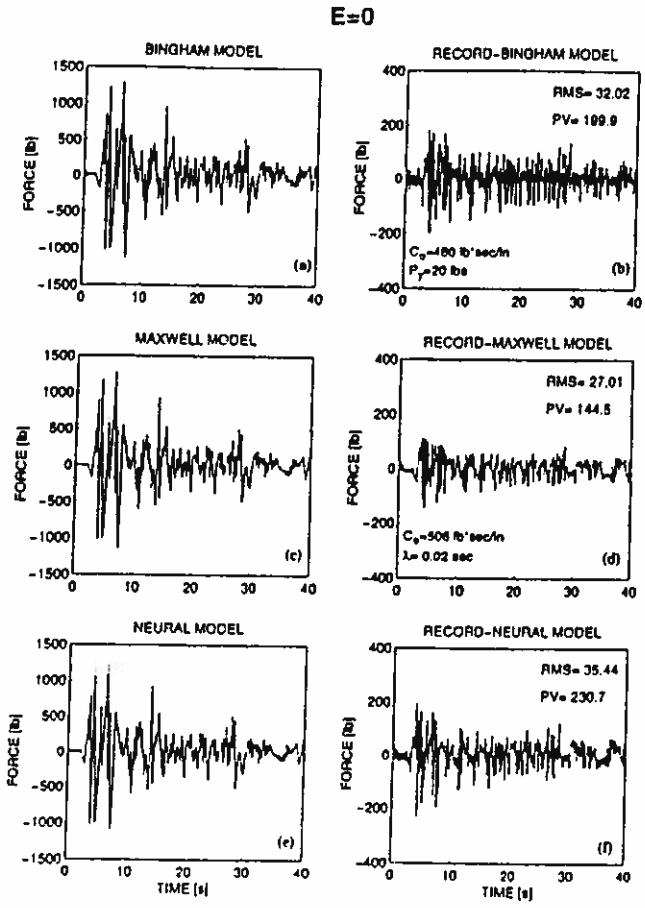

FIG. 9. Comparison of Recorded and Predicted Forces (Left) and Difference Signals (Right) at E = 0 of Bingham Model (Top), Maxwell Model (Center), and Neural Network Model (Bottom) (25.4 mm = 1 in.; 4.448 N = 1 lb)

NEURAL NETWORKS

Neural networks consist of many interconnected simple processing elements called neurons or units, which have multiple inputs and a single output. The inputs are weighted and added together. This sum is then passed through a nonlinearity called the activation function, such as a sigmoidal function like $f(t) = 1/(1 + e^{-t})$ or $f(t) = \tanh(t)$, or a gaussian-type function. The terms "artificial neural networks" or "connectionist models" are typically used to describe these processing units to distinguish them from biological networks of neurons found in living organisms. The processing units or neurons are interconnected and the strength of the interconnections are denoted by parameters called weights. These weights are ad-

justed depending on the task at hand to improve performance. They can be either assigned values via some prescribed off-line algorithm, while remaining fixed during operation, or adjusted via a learning process on-line. Neural networks are classified by network structure topology, by the type of processing elements used, and by the kind of learning rules implemented.

Neural networks are useful as models of dynamical systems because of their ability to be universal function approximators. Several types of neural networks appear to offer promise for use in function approximation. These include the multilayer neural network trained with the back propagation algorithm commonly attributed to Rumelhart et al. (1986), the recurrent neural network such as the feedback network of Hopfield (1982), the content-addressable memory of Kohonen (1980), and the gaussian node network of Moody and Darken (1989). The choice of which neural network to use and which training procedure to invoke is an important decision and varies depending on the intended application. It has been shown that feedforward neural networks can arbitrarily approximate well any continuous function; this, in fact, can be accomplished using a feedforward network with a single hidden layer of neurons with a linear output unit.

Herein, the dependence identification algorithm (DIA), (Moody and Antsaklis 1995), is utilized to construct and train a multilayer neural network to predict the response of the electrorheological damper. The DIA bears some similarities to the boolean network construction algorithm; however, it is designed to work with continuous training problems and it uses the concept of linear dependence, instead of the desired boolean output value, to group patterns together. The algorithm does not share the problems of network pruning techniques because it builds from a small network up to a large one, and because it does not use gradient descent. The DIA is an extremely fast algorithm for function approximation with the advantage that it generates an appropriate network, thus eliminating the need for experimentation to determine the number of hidden neurons. The DIA creates a network and sets of initial conditions that are suitable for further iterative or on-line adaptive training with gradient techniques such as back-propagation.

The DIA utilized displacement-force input-output pairs recorded in the laboratory to construct and train the neural network. The neural network is a single hidden layer network with seven inputs, 99 neurons, one output, and six delays. Displacement histories from three earthquakes have been used as an input to the fluid damper. The resultant force needed to maintain the motion was recorded with the load cell shown in Fig. 1. Fig. 10 plots the three input displacement histories and the recorded forces that we use to train the neural network. The three input seismic records are the 1985 Mexico City earthquakes, the 1987 Whittier Narrows earthquake (Tarzana record), and the 1992 Petrolia earthquake. The center column of plots in Fig. 10 is the recorded force at zero field ($E = 0$) and the right column of plots is the recorded force at 3 kV/mm.

Fig. 9 (bottom-left) compares the prediction of the neural network with the experimentally measured force. The agreement is acceptable, but both PV and RMS values of the dif-

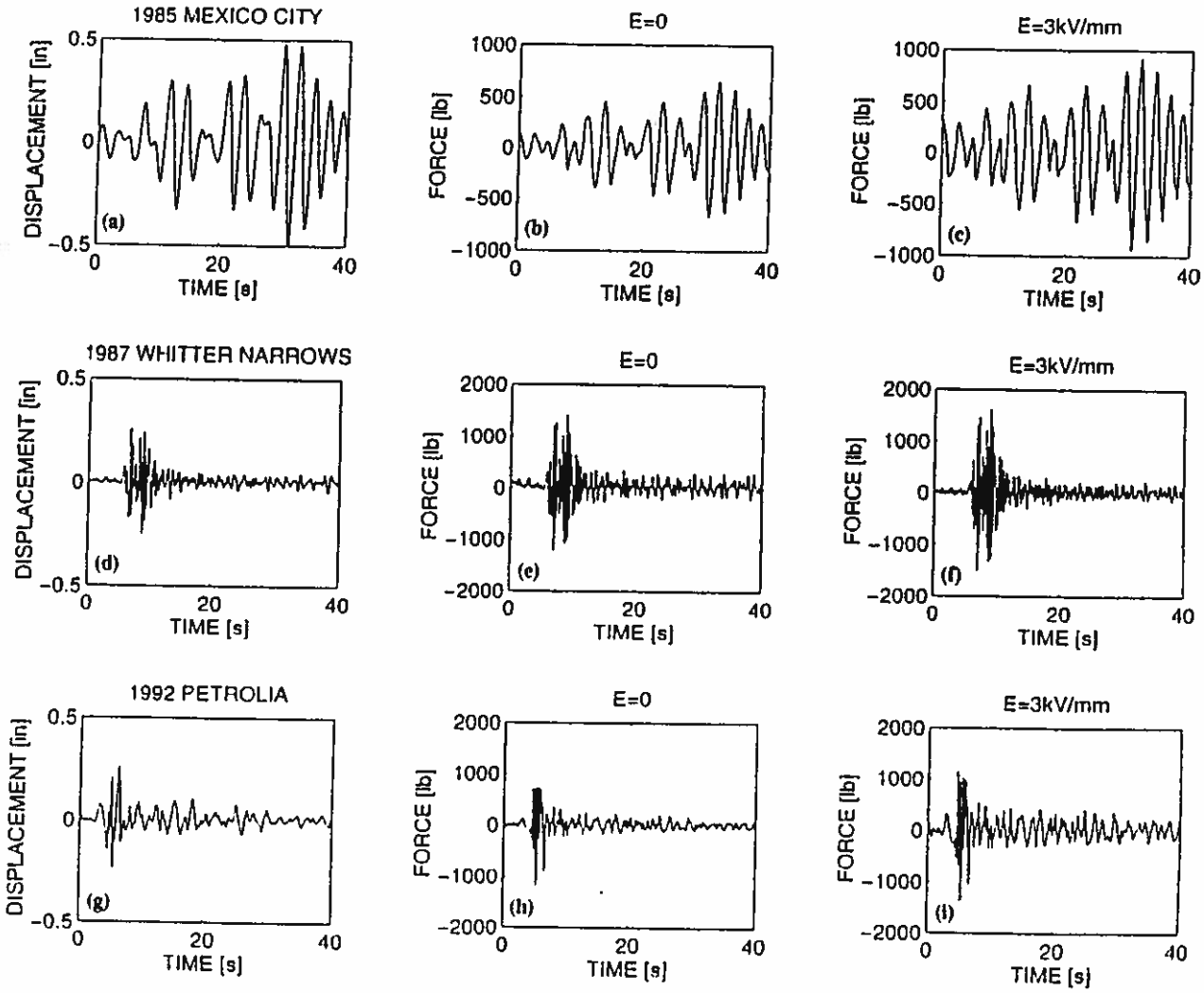

FIG. 10. Recorded Input-Output Signals Used to Train Neural Network

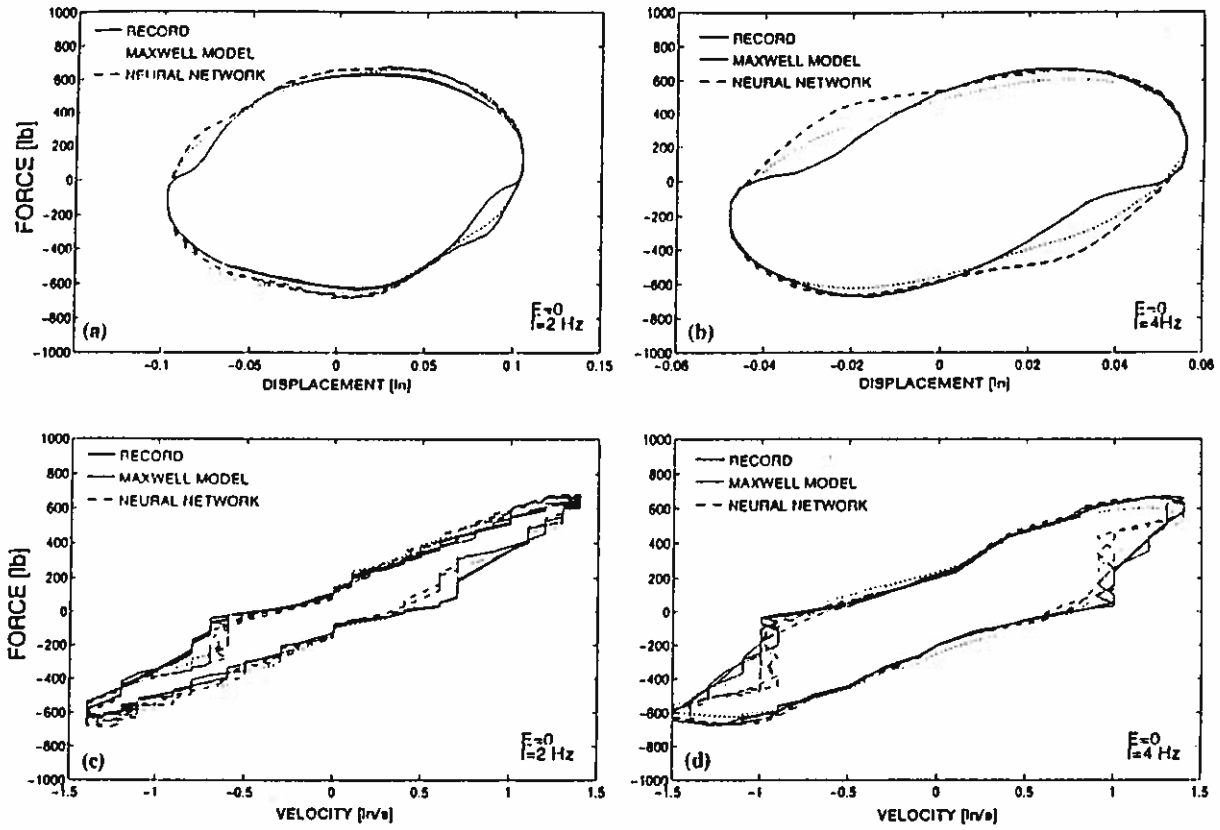

FIG. 11. Comparison of Recorded and Predicted Force-Displacement Loops (Top) and Force-Velocity Loops (Bottom) at $E = 0$; Solid Line: Record; Dotted Line: Maxwell Model; Dashed Line: Neural Network Model (25.4 mm = 1 in.; 4.448 N = 1 lb)

ference signal from the neural network model are larger than the corresponding values resulting from the Bingham and Maxwell models.

To further examine the performance of the DIA-constructed network, the neural network trained with seismic records shown in Fig. 10 was used to predict motions that contain a single harmonic. Fig. 11 compares the recorded (solid line) force-displacement loops (top) and force-velocity loops (bottom) with the predictions of the neural network (dashed line). The predictions of the Maxwell model are also plotted with dots. It is interesting to note that the neural network not only approximates the force-displacement loop but also predicts with success the force-velocity loop, generating a finite area. This means that the neural network model is capable of accounting for the elasticity that the damper manifests as frequency increases.

In the case where the damper is passive (zero field), its response is nearly linear. Figs. 9 and 11 indicate that the simple phenomenological Bingham and Maxwell models surpass the performance of a rather sophisticated neural network. Nevertheless, neural networks may be combined to both identify and control the response of the ER damper therefore creating adaptive controllers. Such adaptive controllers might be useful to address the problem of viscous heating or other time varying effects. Moreover, in the case where electric field is present, the nonlinearities in the damper response become more pronounced and, in this case, the neural network and the DIA become more attractive.

CHARACTERIZATION OF DAMPER RESPONSE UNDER PRESENCE OF ELECTRIC FIELD

Fig. 5 shows recorded force-displacement loops under the presence of electric field (E = 3 kV/mm). These loops depart from the shape of an ellipse and show nonlinear response. A simple phenomenological model that can approximate the nonlinear behavior of the damper under the presence of electric field is again the Bingham model of viscoplasticity, where now the total yield force is the sum of the friction force on the seals, P_f, plus the yield force, P_y, that results from the yielding of the ER material. Accordingly

$$P(t) = (P_y + P_f)\text{sgn}(\dot{u}) + C\dot{u} \tag{7}$$

This macroscopic model was motivated from the mechanical behavior of the ER fluid used within the damper in conjunction with the pattern of flow of the ER fluid through the bypass shown in Figs. 1 and 2. With the assumption that the flow across the bypass is not influenced drastically by the end effects, the pressure drop on the piston head is given by the cubic equation (Phillips 1969; Makris et al. 1996)

$$\Delta p^3 - \left(3\tau_y \frac{L}{h} + \frac{12\eta_0 LQ}{\pi d h^3}\right)\Delta p^2 + 4\tau_y^3 \left(\frac{L}{h}\right)^3 = 0 \tag{8}$$

where Q = flow through the bypass. As the fluid velocity increases, the pressure drop asymptotically reaches the expression

$$\Delta P = \frac{12\eta_0 LQ}{\pi d h^3} + \frac{3L\tau_y}{h} \tag{9}$$

Multiplying (9) with the piston area, A_p, one obtains the yield force, P_y, which can be approximated with the expression

$$P_y \approx \frac{3L\tau_y}{h} A_p \tag{10}$$

Substituting the aforementioned values for the yield stress of the ER fluid and the dimensions of the bypass, the resulting yield force assumes the value of P_y = 267 N ($P_y \approx$ 60 lb).

Fig. 12 (top-left) compares the prediction of the Bingham model given by (7) with the experimental data. Note that in the prediction of the Bingham model the computed value of

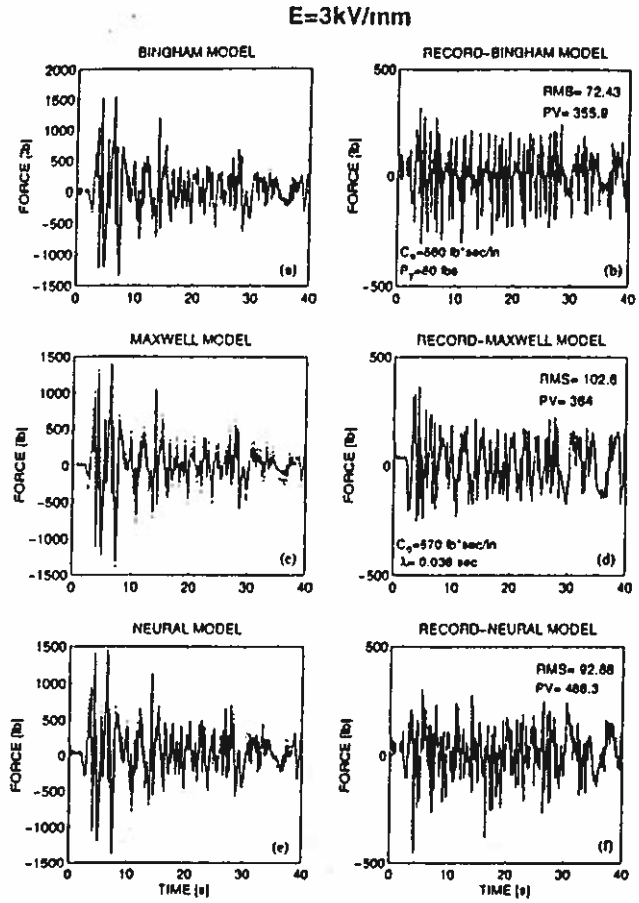

FIG. 12. Comparison of Recorded and Predicted Forces (Left) and Difference Signals (Right) at $E = 3$ kV/mm of Bingham Model (Top), Maxwell Model (Center), and Neural Network Model (Bottom) (25.4 mm = 1 in.; 4.448 N = 1 lb)

$P_y + P_f = 356$ N (80 lb) was used. The difference signal has an RMS = 322.5 kN (72.5 lb) and a PV = 1,583 N (356 lb). Subsequently, the Maxwell model from linear viscoelasticity was utilized to predict the response of the damper at the presence of electric field. To calibrate the parameters of the Maxwell model, oscillatory tests have been conducted under the presence of $E = 3$ kV/mm and the equivalent linear storage stiffness and damping coefficients were extracted using the expressions given by (2). Fig. 13 shows the experimental values and the predictions of the calibrated Maxwell model. The calibrated values for the model parameters are $C = 100$ kN s/m ($C = 570$ lbs s/in.) and $\lambda = 0.036$ s. Fig. 12 (center-left) compares the prediction of the Maxwell model with the experimentally measured force from the damper when subjected to the El-Centro displacement history. Fig. 12 (center-right) shows the difference signal between the predicted and experimentally recorded force histories. It is interesting to note that in this case ($E = 3$ kV/mm), the prediction of the Maxwell model is inferior to the prediction of the Bingham model. This is because under the presence of electric field, the total yield force has increased resulting in a more pronounced nonlinear behavior that cannot be realistically represented with the linear Maxwell model.

Fig. 10 also plots the three input displacement histories and the recorded forces that we used to train the neural network to simulate the damper response under the presence of electric field ($E = 3$ kV/mm). Fig. 12 (bottom-left) compares the prediction of the neural network with the experimentally measured force. The prediction of the neural model is better than the prediction of the Maxwell model in terms of RMS. This shows that neural networks are capable of approximating nonlinear response. Finally, Fig. 14 shows the capabilities of the DIA to predict the response of the damper under the presence of electric field and when subjected to harmonic motions.

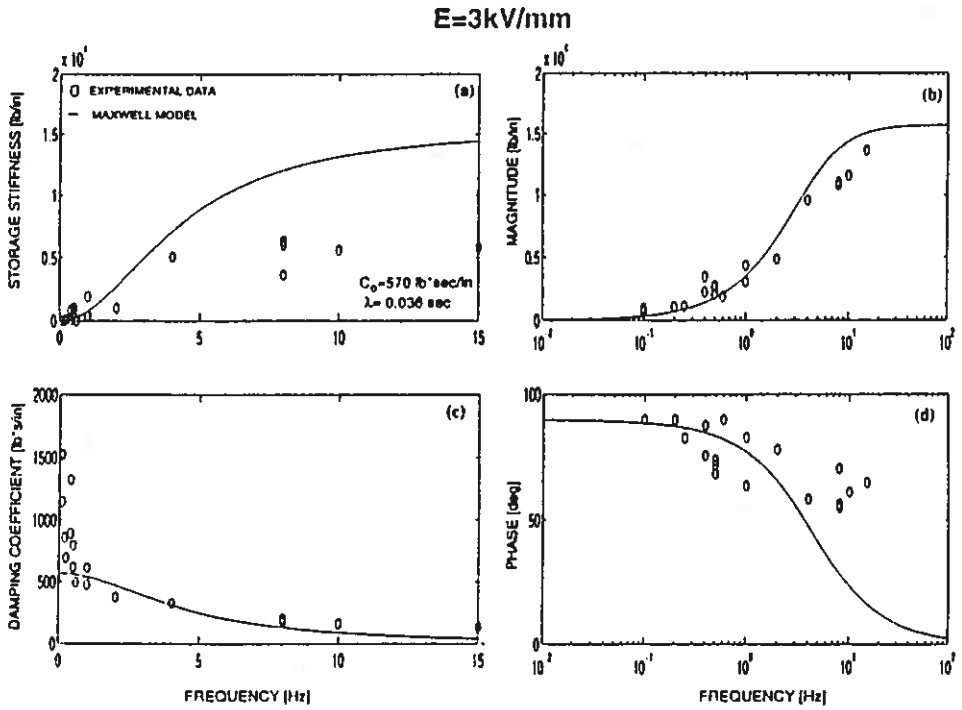

FIG. 13. Experimentally Measured Storage Stiffness and Damping Coefficient (Left), and Magnitude and Phase (Right) of ER Damper as Function of Frequency at $E = 3$ kV/mm (Points); Solid Lines: Prediction of Maxwell Model ($C = 570$ lb s/in.; $\lambda = 0.036$ s; 25.4 mm = 1 in.; 4.448 N = 1 lb)

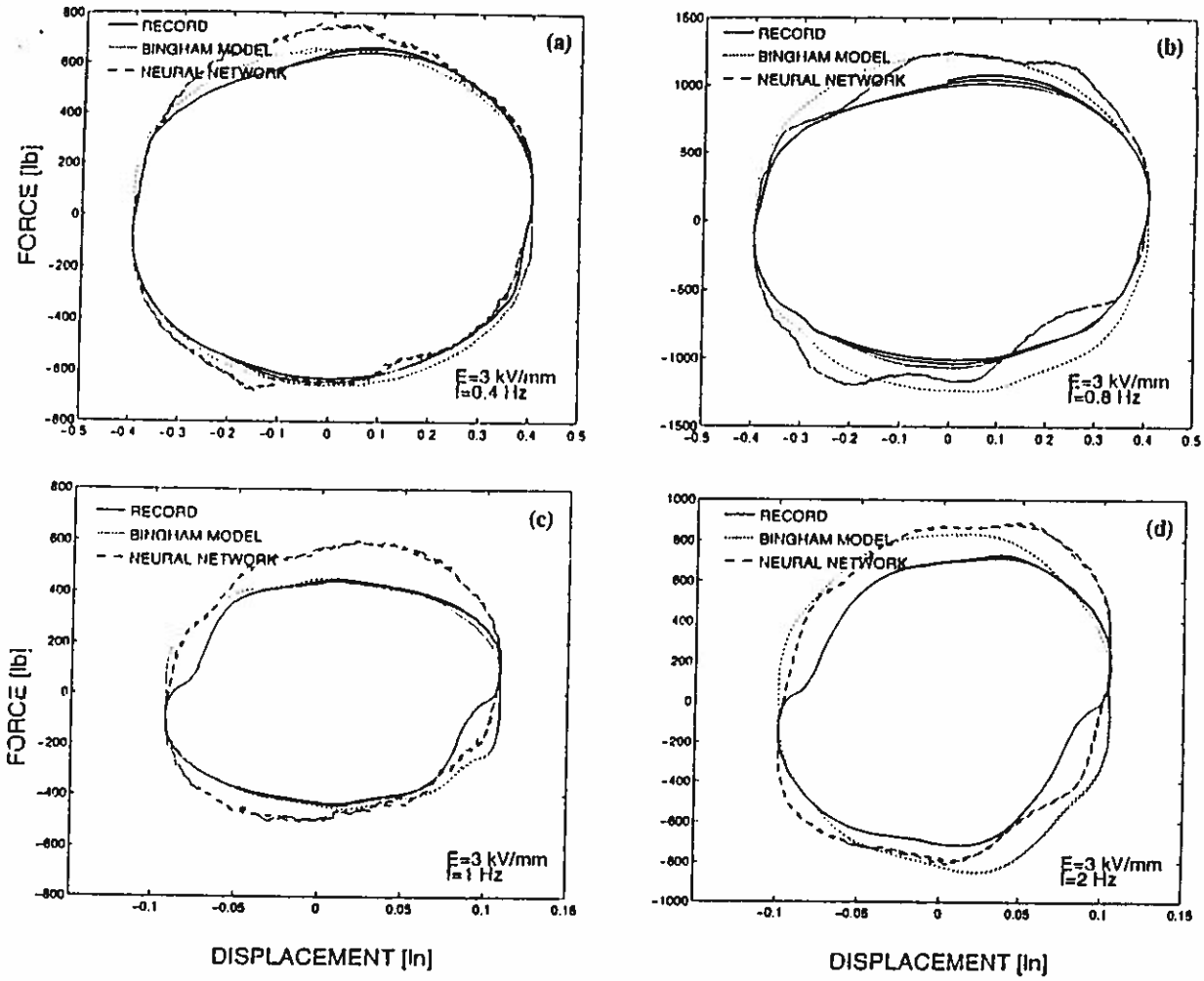

FIG. 14. Comparison of Recorded and Predicted Force-Displacement Loops at $E = 3$ kV/mm; Solid Line: Dotted Line: Maxwell Model; Dashed Line: Neural Network Model (25.4 mm = 1 in.; 4.448 N = 1 lb)

CONCLUSIONS

In the present paper the performance of physically motivated phenomenological models and neural networks has been examined when predicting the measured response of an ER semiactive damper. It was found that a neural network constructed with the dependence identification algorithm predicts satisfactorily the response of the damper without and with the presence of electric field. Specifically, under the presence of electric field, where a more pronounced nonlinear response prevails, the predictions of the neural network are comparable but not superior to the predictions of simple phenomenological models. It was also found that although the trained neural network is capable of approximating the damper response subjected to harmonic motions it performs better in predicting the damper response when subjected to random signals.

Although at this stage the performance of the proposed neural network does not surpass the performances of elementary phenomenological models, neural networks may be combined to both identify and control the response of the semiactive damper, therefore creating adaptive controllers. Such adaptive controllers might be useful to address the problem of viscous heating or other time varying effects. Future studies will investigate the performance of neural networks to approximate the damper response during time varying electric field and temperature.

ACKNOWLEDGMENTS

This work is supported by the National Science Foundation Grant BCS-9300827. The main cylinder of the damper was manufactured and donated by Taylor Devices, Inc. N. Tonawanda, N.Y. Professor D. Hill, and Ms. M. Jordan manufactured the ER fluid. Special thanks to Mr. Richard Strebinger for helping with the construction of the ER bypass and to Mr. J. Moody for helping with the dependence identification algorithm.

APPENDIX I. REFERENCES

Block, H., and Kelly, J. P. (1988). "Electrorheology." *J. Appl. Phys.*, 21, 1661–1677.

Constantinou, M. C., and Symans, M. D. (1993). "Seismic response of structures with supplemental damping." *Struct. Design Tall Build.*, 2, 77–92.

Douclos, T. G. (1988). "Electrorheological fluids and devices." *Automotive Engrg.*, 96, 45–48.

Ehrgott, R. C., and Masri, S. F. (1992). "Modeling the oscillatory dynamic behavior of electrorheological materials in shear." *Smart Mat. and Struct.*, 1, 275–285.

Franklin, G. F., Powell, J. D., and Emani-Naeini, A. (1991). *Feedback control of dynamic systems*. Addison-Wesley Publications, Inc., Reading, Mass.

Gamota, D. R., and Filisko, F. E. (1991). "Dynamic mechanical studies of electrorheological materials: moderate frequencies." *J. Rheology*, 35, 399–425.

Gamota, D. R., Wineman, A. S., and Filisko, F. E. (1993). "Fourier transform analysis: nonlinear dynamic response of an electrorheological material." *J. Rheology*, 37, 919–933.

Gavin, H. P., and Hanson, R. D. (1994a). "Characterization of an ER active member." *Proc., Struct. Congr. XII*, Baker and Goodno, eds., ASCE, New York, N.Y. 2, 863–868.

Gavin, H. P., and Hanson, R. D. (1994b). "Electrorheological dampers for structural vibration suppression." *Rep. No. UMCEE 94-35*, Dept. Civ. and Envir. Engrg., Univ. of Michigan, Ann Arbor, Mich.

Ghaboussi, J., and Joghataie, A. (1995). "Active control of structures using neural networks." *J. Engrg. Mech.*, ASCE, 121(4), 555–567.

Hopfield, J. J. (1982). "Neural networks and physical systems with emergent collective computational abilities." *Proc., Nat. Acad. of Sci.*, 79, 2554–2558.
Housner, G. W., Soong, T. T., and Masri, S. F. (1994). "Second generation of active structural control in civil engineering." *Proc., 1st World Conf. Struct. Control*, Int. Assn. for Struct. Control, Los Angeles, Calif., 1, 3–18.
Jordan, T. C., and Shaw, M. T. (1989). "Electrorheology." *IEEE Trans. Electr. Insulation*, 24, 849–878.
Kawashima, K., and Unjoh, S. (1994). "Seismic response control of bridges by variable dampers." *J. Struct. Engrg.*, ASCE, 120(9), 2583–2601.
Kohonen, T. (1980). *Content-addressable memories*, Springer-Verlag, New York, N.Y.
Makris, N., and Constantinou, M. C. (1991). "Fractional-derivative maxwell model for viscous dampers." *J. Struct. Engrg.*, ASCE, 117(9), 2708–2724.
Makris, N., Dargush, G. F., and Constantinou, M. C. (1993). "Dynamic analysis of generalized viscoelastic fluids." *J. Engrg. Mech.*, ASCE, 119(8), 1663–1679.
Makris, N., Dargush, G. F., and Constantinou, M. C. (1995a). "Dynamic analysis of viscoelastic fluid dampers." *J. Engrg. Mech.*, ASCE, 121(10), 1114–1121.
Makris, N., Hill, D., Burton, S., and Jordan, M. (1995b). "Electrorheological fluid damper for seismic protection of structures." *Proc., SPIE, Smart Structures and Mat.*, I. Chopra, ed., The Int. Soc. of Optical Engrg., Bellingham, Wash., 2443, 184–194.
Makris, N., Burton, S., Hill, D., and Jordan, M. (1996). "Analysis and design of an electrorheological damper for seismic protection of structures." *J. Engrg. Mech.*, ASCE, 122(10).
Masri, S. F., Ghassiakos, A. G., and Caughey, T. K. (1993). "Identification of nonlinear dynamic systems using neural networks." *J. Appl. Mech.*, 60, 123–133.
Moody, J. O., and Antsaklis, P. J. (1995). "The dependence identification neural network construction algorithm." *Trans. on Neural Networks, IEEE*, New York, N.Y.
Moody, J. O., and Darken, D. J. (1989). "Fast learning in networks of locally-tuned processing units." *Neural Computation*, 1, 281–294.
Patten, W. N., Sack, R. L., and He, Q. (1994). "Suppression of vehicle-induced bridge vibration via a semiactive structural controller." *Proc., 1st World Conf. Struct. Control*, Int. Assn. for Struct. Control, Los Angeles, Calif., 3, FA2-83–FA2-90.
Poincare, H. (1929). *The foundation of science*, Science, New York, N.Y.
Phillips, R. W. (1969). "Engineering Applications of Fluids with Variable Yield Stress," PhD dissertation, Univ. of California, Berkeley, Calif.
Schlichting, H. (1987). *Boundary-layer theory*, McGraw-Hill Book Co., Inc., New York, N.Y.
Rumelhart, D. E., Hinton, G. E., and Williams, R. J. (1986). "Learning internal representations by error propagation," Rumelhart and McClelland, eds., *Parallel distributed processing: explorations in the microstructure of cognition, vol. 1: foundation*, MIT Press, Cambridge, Mass., 318–362.
Shames, I. H., and Cozzarelli, F. A. (1992). *Elastic and inelastic stress analysis*, Prentice-Hall, Inc., Englewood Cliffs, N.J.
Stevens, N. G., Sproston, J. L., and Stanway, R. (1984). "Experimental evaluation of a simple electroviscous damper." *J. Electrostatics*, 15, 275–283.
Symans, M., and Constantinou, M. C. (1995). "Development and experimental study of semi active fluid damping device for seismic protection of structures." *Rep. NCEER-950011*, Nat. Ctr. for Earthquake Engrg. Res., Buffalo, N.Y.
Tung, A. T., Wong, F. S., and Dong, W. (1994). "Prediction of the spatial distribution of the modified mercalli intensity using neural networks." *Earthquake Engrg. and Struct. Dyn.*, 23, 49–62.
Winslow, W. M. (1949). "Induced fibration of suspensions." *Appl. Phys.*, 20, 1137–1140.

APPENDIX II. NOTATION

The following symbols are used in this paper:

A_p = area of piston head;
C = small-velocity damping constant;
d = diameter of bypass;
E = electric field;
h = width of gap along ER duct;
L = length of bypass;
p = pressure;
Q = flow rate;
r = radial distance;
t = time;
Δp = pressure drop on piston head;
Δp_v = pressure drop on piston head due to viscous stresses only;
η_0 = zero-shear rate viscosity;
λ = relaxation time;
π = 3.14159...;
τ_y = yield stress of ER material;
ω = angular frequency.